

Mesoporous carbon synthesized from sewage sludge and its electrochemical properties

Jonggil Kwon, Kue-Ho Kim, Hyo-Jin Ahn and Yeon Hwang*

Department of Materials Science and Engineering, Seoul National University of Science and Technology, Seoul 01811, South Korea

Activated carbon having high specific surface area was synthesized from sewage sludge by acid treatment and KOH activation process, and its electrochemical properties were measured to research the potential use as electrode material. All activated sludge samples were synthesized as graphitic-like phase. The optimum activation condition, where the specific surface area, cyclic voltametry (CV) characteristics and capacitance showed the best values, was at the weight ratio of $W_{\text{KOH}}/W_{\text{sludge}} = 3.5/1$. Mesoporous carbon synthesized at this condition showed $1,617 \text{ m}^2\text{g}^{-1}$ of specific surface area and 134.6 Fg^{-1} of specific capacitance at the current density of 0.2 Ag^{-1} . High specific surface area resulted in the high specific capacitance.

Keywords: Sewage sludge, Mesoporous, KOH activation, Activated carbon.

Introduction

Most of the developing countries that experienced industrialization and civilization in a short period had suffered a rapid water pollution of rivers and public water. It was no wonder that the large amount of sewage water became social issues. To improve the water quality lots of sewage water purification plants have been constructed, which also resulted in the massive production of sewage sludges. The sewage sludge means a sedimented waste separated from a complex liquid phases of sewage water [1, 2]. It is composed of various kinds of inorganic and organic phases with large amount of water. The composition of the sludge is not fixed, and varies in a large scale according to the produced local area and processing season. For example, the sludges that were produced in Seoul, Korea consist of 1.2-13.0 wt.% of fixed carbon, 10.0-70.3 wt.% of volatiles, 22.2-67.7 wt.% of ash, and 78-80 wt.% of water in a quantitative analysis. In an ultimate analysis, they consist of 15.5-44.8 wt.% of carbon, 2.3-7.6 wt.% of hydrogen, 1.8-6.4 wt.% of nitrogen, 13.9-23.1 wt.% of oxygen, and 0-1.5 wt.% of sulfur [3-6].

There are two major approaches for sludge treatments. The first one is the sludge reuse such as biosolids for land soil [7, 8], carbonization [9, 10], assisted fuel for cement production and/or coal power plants [11, 12], and structural components [13-16]. The second one is

the reducing the weight of sludge by physical, chemical and biological treatments [17]. In this paper we tried to convert dried sewage sludge into activated carbon having high specific surface area. If we adopt appropriate carbonization process, it is expected to be able to synthesis activated carbon because the sludge has some amount of carbon. We adopted KOH activation process [18, 19] to produce mesoporous carbon. It is known that mesoporous carbon has successfully been synthesized from precursors like ecklonia cava and tofu using KOH activation [20-22]. Mesoporous carbon was successfully synthesized by the activation of dried sewage sludge, and its electrochemical properties were examined to search for the use for electrode material.

Experimental Procedure

Synthesis

The mesoporous carbon was synthesized from sewage sludge by alkali activation process. The wet sludge was firstly dried by putting it in a open field for several days to reduce the water content and remove bad odors. Subsequent hot-air drying at $180 \text{ }^\circ\text{C}$ for 1 h reduced the water content of the sludge from 46.0 wt.% to 9.2 wt.%. The dried sludge was washed by nitric acid, followed by the heat treatment in ambient atmosphere at $400 \text{ }^\circ\text{C}$ for 3 h to eliminate organics and impurities, which led to the stabilization of the sludge sample. The purified sludge sample was washed several times by de-ionized (DI) water, and dried at $100 \text{ }^\circ\text{C}$. It was mixed with potassium hydroxide (KOH, Samchun Chemical), and the mixture was carbonized at $800 \text{ }^\circ\text{C}$ for 2 h in a nitrogen atmosphere. This is the KOH activation process. The weight ratio of the KOH and sludge ($W_{\text{KOH}}/$

*Corresponding author:
Tel : +82-2-970-6517
Fax: +82-2-973-6657
E-mail: yhwang@seoultech.ac.kr

W_{sludge}) was varied as 2.5/1, 3.0/1, 3.5/1 and 4.0/1. The activated sample was washed by hydrochloric acid (HCl, Samchun Chemical) and DI water to eliminate any residues incorporated from the activation process. Final activated carbon sample was obtained by drying at 80 °C.

Characterization

The thermal decomposition and heat evolution was determined by thermogravimetry (TG) and differential thermal analysis (DTA, Shimadzu DTG-60). It was done in ambient atmosphere at the 50 mLmin⁻¹ of the air flow from 25 °C up to 1300 °C at the 10 °Cmin⁻¹ of heating rate. Structural and phase analysis was conducted using x-ray diffractometer (XRD, Bruker DE/D8 Advance). It was done from 20° to 80° of two-theta with the scan speed of 5 °min⁻¹ using Cu Ka radiation. The morphology of the sample was observed using scanning electron microscopy (SEM, Carl Zeiss EVO10). The pore structure was determined using Brunauer-Emmett-Teller (BET) and Barrett-Joyner-Halenda (BJH) (BELSORP-mini II) methods with the N₂ adsorption-desorption isotherms.

Electrochemical analysis

Electrochemical properties of the activated sludge were measured by two-electrode system with 6 M KOH solution as the electrolyte. The electrode paste was prepared using mesoporous activated carbon as an active material, Ketjenblack (Mitsubishi Chemical, ECP-600JD) as a conducting material, and polyvinylidene difluoride (PVDF, Alfa Aesar) in N-methyl-2-pyrrolidone (Aldrich, NMP 99.5%) as a binder. CV was done in the potential range of 0-1.0 V using a potentiostat-galvanostat (Ecochemie Autolab, PSGT302N) at the scan rate of 10 mVs⁻¹. The charging-discharging characteristics were tested at the current density of 0.2-2.0 Ag⁻¹. The specific capacitance was obtained from a discharge curve using the following equation,

$$C_{\text{sp}} = 4I/(m\text{dV}/\text{dt}) \quad (1)$$

where I (A), m (g), V (V) and t (s) are charging-discharging current, total mass of the activated sludge, voltage drop upon discharging and total discharging time, respectively. Nyquist plot was obtained using a potentiostat-galvanostat at the frequency response analyzer (FRA) impedance potentiostatic mode in the frequency range of 10⁻²-10⁵ Hz.

Results and Discussion

Fig. 1 shows the TG and DTA results of the dried sludge. The endothermic peak at 110.1 °C represents the water evaporation, which leads to 8% of weight decrease. The large exothermic peak at 389.1 °C results from the oxidation of the organic ingredients of the

sludge. Above this temperature, the sludge undergoes 32% of weight decrease. The thermal analysis suggests that the heat treatment at 400 °C is sufficient to eliminate organics and/or impurities from the sludge.

Fig. 2 shows the XRD patterns of the sludge. In Fig. 2(a), we can see the phases of the dried and acid treated sewage sludge. In the figure, the symbols of K,

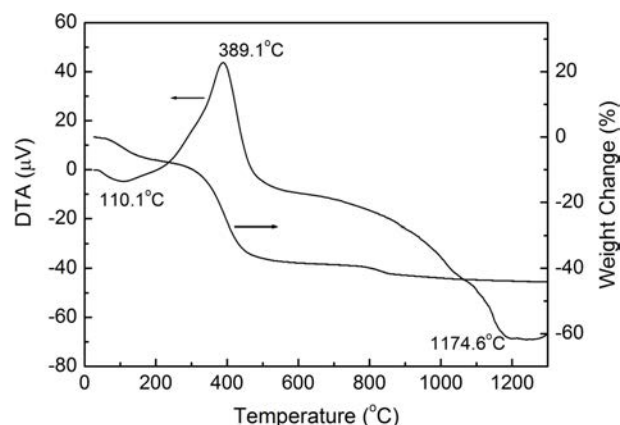


Fig. 1. Thermogravimetry and differential thermal analysis of dried sewage sludge.

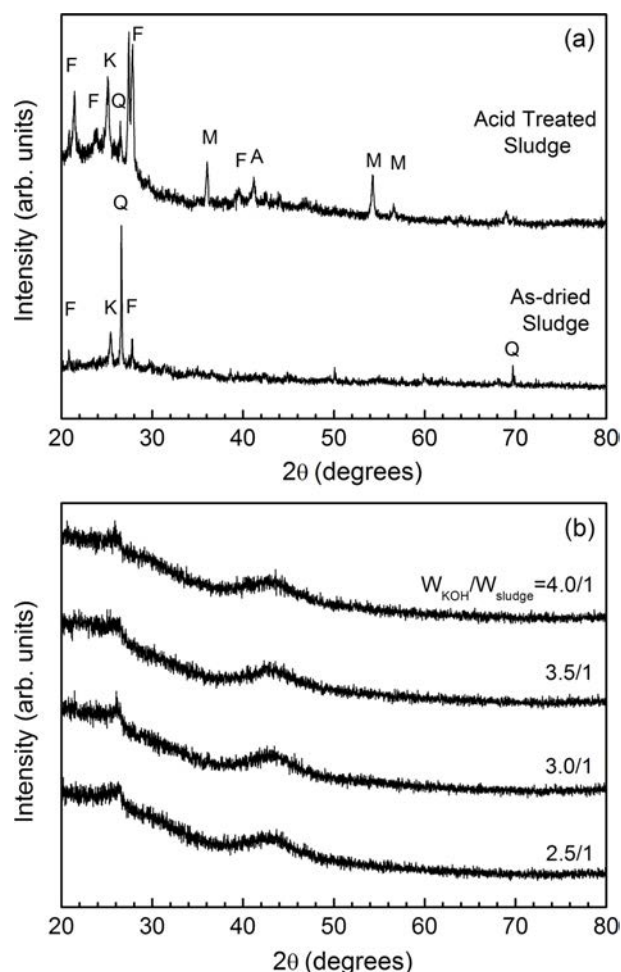


Fig. 2. X-ray diffraction patterns of (a) dried and acid-treated sewage sludge, and (b) KOH activated carbon.

F, Q, M and A denote kaolinite, sodium feldspar, quartz, magnetite and α -alumina, respectively. The as-dried sludge consists of kaolinite, feldspar and quartz. After the acid treatment magnetite and alumina, which are veiled by other phases before treatment, appear. Fig. 2(b) is the XRD patterns of the KOH activated samples. All samples, regardless of the $W_{\text{KOH}}/W_{\text{sludge}}$ ratio, shows diffraction peaks at 26° and 43° of two-theta. These correspond to (002) and (101) planes of graphite, respectively [23, 24]. The intensities of two peaks, which represent the crystallinity of graphite, do not vary according to the $W_{\text{KOH}}/W_{\text{sludge}}$ ratio. This suggests that

KOH activation converts sludge into graphitic phase.

Fig. 3 shows SEM photographs of sludges. From Fig. 3(a) and (b), it is seen that the surfaces of as-dried and acid treated samples do not have pore structures. The starting material, i.e. the as-dried sludge, is composed of lump particles with smooth surfaces. After KOH activation, pores of various sizes are observed (Fig. 3(c)-(f)). As the weight ratio of KOH and sludge increases it is seen that small pores as well as large ones are developed. However, it is known that excess alkali activation leads to the decrease of the number of pores, and there exists optimum activation concentration

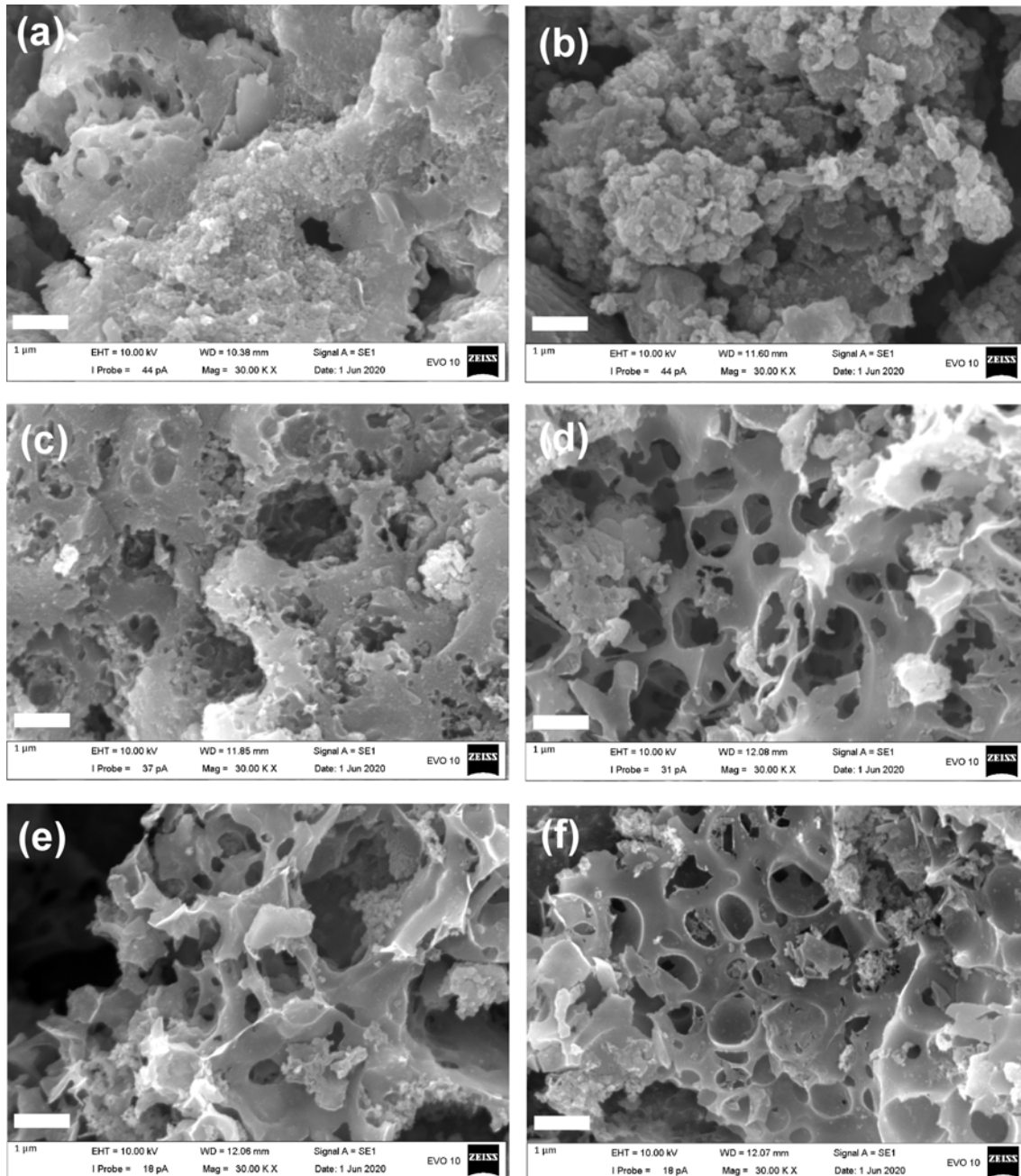


Fig. 3. Scanning electron microscopy photographs of the sludge samples. (a) Dried sludge, (b) acid-treated sludge, (c) KOH activated carbon at $W_{\text{KOH}}/W_{\text{sludge}} = 2.5/1$, (d) $W_{\text{KOH}}/W_{\text{sludge}} = 3.0/1$, (e) $W_{\text{KOH}}/W_{\text{sludge}} = 3.5/1$, and (f) $W_{\text{KOH}}/W_{\text{sludge}} = 4.0/1$. All scale bars are 1 μm .

to maximize the pore development [25].

To examine the pore structures of KOH activated carbon, nitrogen adsorption-desorption isotherms were measured and the results are summarized at Fig. 4 and Table 1. Fig. 4 is the BET and BJH plots of KOH activated samples. According to the IUPAC (International Union of Pure and Applied Chemistry), pores are classified as micropore (< 2 nm), mesopore (2-50 nm) and macropore (>50 nm) [26-28]. In Fig. 4(a) all isotherms of KOH activated sludges show Type-IV adsorption-desorption behavior, which suggests that the mesopore structures have been developed at high N_2 pressure ($p/p_0 > 0.45$). It is seen from Fig. 4(b) that the activated carbon showed distinctive isotherm behavior of mesoporous structures, having 23 and 44 nm of pore size. KOH activation was successful to develop the mesoporous carbon structure. Overall, all samples of KOH activation showed mesoporous carbon structures. Table 1 summarizes the BET analysis of the porous structures. The specific surface area increases according to the increase of the W_{KOH}/W_{sludge} ratio, and it is maximum at $W_{KOH}/W_{sludge} = 3.5/1$. Total pore volume and average pore diameter are also highest at $W_{KOH}/W_{sludge} = 3.5/1$.

The electrochemical properties of the mesoporous

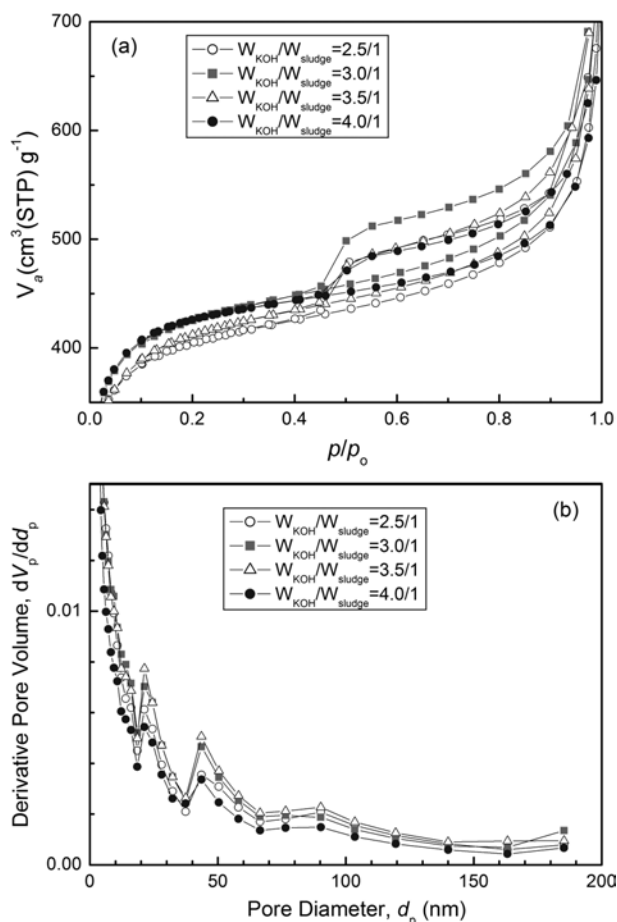


Fig. 4. (a) Nitrogen adsorption-desorption isotherms, and (b) BJH pore size distribution of KOH activated carbon.

carbon were investigated by measuring the CV and capacitance characteristics. As shown in Fig. 5, all KOH activated carbon samples show rectangular CV curves with good symmetry, which implies the presence of the electrical double layer region at the interface between electrode and electrolyte. The largest CV curve was obtained at $W_{KOH}/W_{sludge} = 3.5/1$, and it was attributed to the largest specific surface area and large electrical double layer region. Fig. 6 shows the specific capacitance of activated carbon measured from the charging-discharging tests. Samples show 116.6-134.6 Fg^{-1} of specific capacitance at the current density of

Table 1. Specific surface area, total pore volume and average pore diameter of the KOH activated carbon.

| W_{KOH}/W_{sludge} ratio | S_{BET} (m^2g^{-1}) | Total pore volume, $p/p_0=0.990$ (cm^3g^{-1}) | Average pore diameter (nm) |
|----------------------------|---------------------------|---|----------------------------|
| 2.5/1 | 1519 | 1.0557 | 2.78 |
| 3.0/1 | 1610 | 1.1293 | 2.81 |
| 3.5/1 | 1617 | 1.1321 | 2.93 |
| 4.0/1 | 1544 | 1.0092 | 2.49 |

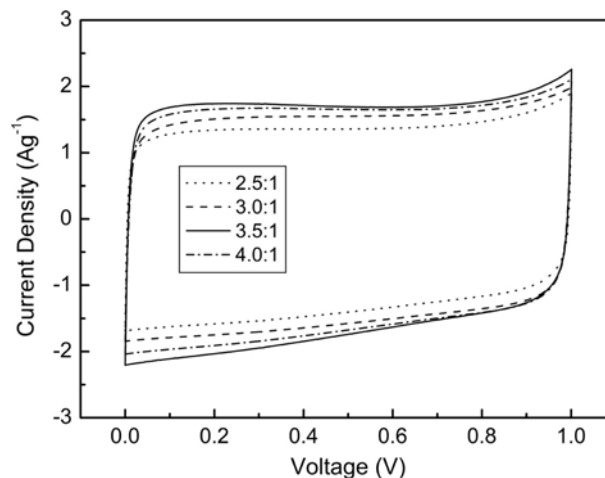


Fig. 5. Current-potential characteristics of KOH activated carbon.

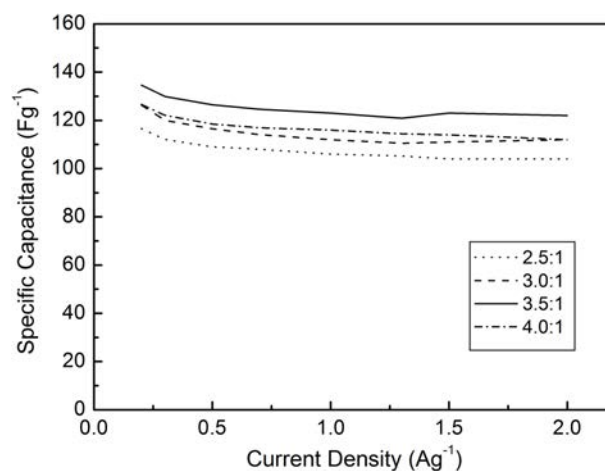
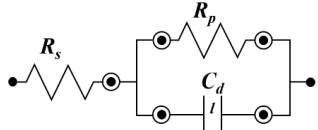


Fig. 6. Specific capacitance-current characteristics of KOH activated carbon.

Table 2. Simplified equivalent circuit and simulated parameters of KOH activated mesoporous carbon. R_s , R_p and C_{dl} imply the series resistance, the parallel resistance and the capacitance, respectively.

| Equivalent Circuit | $W_{\text{KOH}}/W_{\text{sludge}}$ ratio | R_s (m Ω) | R_p (m Ω) | C_{dl} (μF) |
|---|--|---------------------|---------------------|----------------------------|
|  | 2.5/1 | 456 | 419 | 289 |
| | 3.0/1 | 519 | 412 | 329 |
| | 3.5/1 | 518 | 460 | 340 |
| | 4.0/1 | 525 | 395 | 336 |

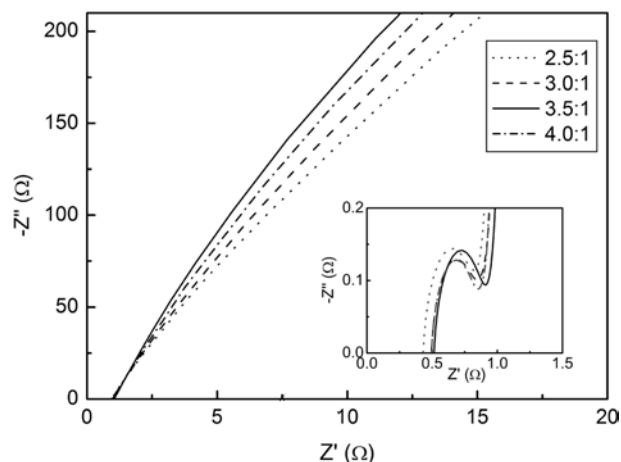


Fig. 7. Nyquist plots of KOH activated carbon.

0.2 Ag^{-1} . This relatively high capacitance originates from high specific surface area. It is natural that the largest capacitance is obtained at $W_{\text{KOH}}/W_{\text{sludge}} = 3.5/1$, which is the activation condition showing maximum specific surface area. The mesoporous microstructure increased the wettability between the electrolyte and carbon, which enhanced the formation of the electric double layer.

Nyquist plots of the activated carbon are shown in Fig. 7. All data exhibit typical AC impedance characteristics of supercapacitors [29]. At the high frequency range (the inset of Fig. 7) where the electrode exhibits inner resistance, each carbon electrodes showed different curves. A small semicircle in the high frequency region is the dominant resistive nature of the supercapacitor system consisting of electrode/electrolyte/current-collector [30, 31]. The real axis intercept at the left side of the semicircle is the equivalent series resistance. It originates from the electrolyte solution and electrode material, depending on the ionic concentration, type of ions, temperature and the geometry of the contact region between the electrolyte and electrode. The difference between the left-intercept and right-intercept of semicircle, i.e. the diameter of the semicircle, corresponds to the equivalent parallel resistance. This is related with the electrode conductivity and the charge-transfer resistance of electrode materials. The speed of the charge transfer reaction depends on the concentration of the reaction products. The plots were fitted using simplified equivalent

circuit model including the series and parallel resistances and the capacitance of the electric double layer. The results are shown in Table 2 along with the equivalent circuit. The electrode at the $W_{\text{KOH}}/W_{\text{sludge}} = 3.5/1$ condition showed the largest capacitance of electric double layer. The equivalent series and parallel resistances were high on the whole at this condition.

The sharply increasing straight line at the low frequency range in Fig. 7 represents the capacitive behavior of the ionic charges at the pore surfaces [32]. At this frequency range, the ions can more easily diffuse into the pores. The steepest slope appears at $W_{\text{KOH}}/W_{\text{sludge}} = 3.5/1$. Because the ion diffusion was enhanced owing to the shorter diffusion paths at the mesoporous surfaces, the electrode behaved as an optimized interface which leads to a steep line in the Nyquist plot.

Conclusions

In summary, we synthesized mesoporous activated carbon from sewage sludge by acid treatment and KOH activation processes. All activated sludge samples were synthesized as graphitic phase. The optimum activation condition, where the properties of carbon such as the specific surface area, CV and capacitance showed the best values, was $W_{\text{KOH}}/W_{\text{sludge}} = 3.5/1$. At this synthesis condition mesoporous carbon showed $1,617 \text{ m}^2\text{g}^{-1}$ of specific surface area and 134.6 Fg^{-1} of specific capacitance at the current density of 0.2 Ag^{-1} . High specific capacitance occurred because of the high specific surface area. The mesoporous structure offered a good path for ion diffusion within a short range. Overall, the mesoporous activated carbon that was synthesized by KOH activation process of sewage sludge could be a good candidate for high-performance electrical double layer capacitors.

Acknowledgement

This study was supported by the Research Program funded by Seoul National University of Science and Technology (2020-0588).

References

1. L.E. Stommers, D.W. Nelson and K.J. Yost, *J. Environ. Quality* 5 (1976) 303.

2. L.E. Stommers, *J. Environ. Quality* 6 (1977) 225.
3. W. Cho, J.Y. Kim, J.J. Lee and J.-Y. Lee, *J. Korea Soc. Waste Manag.* 37 (2020) 295.
4. S.-Y. Lee, S.-W. Park, Y.-O. Jeung, G.-H. Han, Y.-C. Seo and W.-H. Kim, *J. Korea Soc. Waste Manag.* 36 (2019) 608.
5. S.-C. Jung, M.-S. Shin and Y.-W. Jeon, *J. Korea Soc. Waste Manag.* 35 (2018) 507.
6. D. Oh, D. Kim, H.W. Song, H. Kim and K.Y. Park, *J. Korea Soc. Waste Manag.* 34 (2017) 56.
7. T.K. Graczyk, M. Kacprzak, E. Neczaj, L. Tamang, H. Graczyk, F.E. Lucy and A.S. Girouard, *Environ. Res.* 106 (2008) 27.
8. Q. Li, Z. L. He and P. J. Stoffella, *Appl. Environ. Soil Sci.* 2012 (2012) 11.
9. T. Yoshida and M. J. Antal Jr., *Energy Fuels* 23 (2009) 5454.
10. N.-Y. Wang, C.-H. Shih, P.-T. Chiueh and Y.-F. Huang, *Energies* 6 (2013) 871.
11. S.S.A.S. Hassan, Y. Wang, S. Hu, S. Su and J. Xiang, *Renew. Sustain. Energy Rev.* 80 (2017) 888.
12. A. Dominguez, J.A. Menéndez, M. Inguanzo and J.J. Pis, *Bioresource Tech.* 97 (2006) 1185.
13. X.D. Spiliotisa, K.I. Ntampeglitisa, V.G. Karayannisb and G.A. Papapolymerou, *J. Ceram. Process. Res.* 16 (2015) 11.
14. Z.X. Yanga, N.R. Haa, M.S. Janga, K.H. Hwanga and J.K. Lee, *J. Ceram. Process. Res.* 10 (2009) 266.
15. A. Koenig and J. N. Kay, *Proc. 3rd Inter. Symp. Environ. Geotech.* (1996) 73.
16. J.E. Alleman and A.B. Neil, *J. Environ. Eng.* 110 (1084) 301.
17. E.W. Steel and T.J. McGhee, in "Water Supply and Sewerage, 5th Ed." (McGraw-Hill, 1979) p.533-534.
18. T. Otowa, R. Tanibata and M. Itoh, *Gas Sep. Purif.* 7 (1993) 241.
19. H. Zhang, Z. Mo, R. Guo, N. Liu, M. Yan, R. Wang, H. Feng and X. Wei, *J. Mater. Res.* 15 (2019) 1200.
20. K.-H. Kim, D.-Y. Shin and H.-J. Ahn, *J. Ind. Eng. Chem.* 84 (2020) 393.
21. D.-Y. Lee, G.-H. An and H.-J. Ahn, *J. Ind. Eng. Chem.* 52 (2017) 121.
22. G.-H. An, D.-Y. Lee and H.-J. Ahn, *J. Ind. Eng. Chem.* 65 (2018) 423.
23. Z.Q. Li, C.J. Lu, Z.P. Xia, Y. Zhou and Z. Luo, *Carbon* 45 (2007) 1686.
24. A. Sayaha, F. Habelhamesa, A. Bahloula, B. Nessarka, Y. Bonnassieuxb, D. Tendelierb and M. El Jouadc, *J. Electroanal. Chem.* 818 (2018) 26.
25. D.-Y. Lee, G.-H. Ahn and H.-J. Ahn, *J. Ind. Eng. Chem.* 52 (2017) 121.
26. E. Raymundo-Piñero, F. Leroux and F. Béguin, *Adv. Mater.* 18 (2006) 1877.
27. C. Largeot, C. Portet, J. Chmiola, P.-L. Taberna, Y. Gogotsi and P. Simon, *J. Am. Chem. Soc.* 130 (2008) 2730.
28. B.-W. Jo, J.-S. Choi and S.-W. Kang, *J. Ceram. Process. Res.* 12 (2011) 294.
29. D.Y. Qu, *J. Power Sources* 109 (2002) 403.
30. J. Gamby, P.L. Taberna, P. Simon, J.F. Fauvarque and M. Chesneau, *J. Power Sources* 101 (2001) 109.
31. J. Chmiola, G. Yushin, R. Dash and Y. Gogotsi, *J. Power Sources* 158 (2006) 765.
32. W.C. Chen, T.C. Wen and H. Teng, *Electrochim. Acta* 48 (2003) 641.